

Lindenane-Based Sesquiterpenoid Hetero-Oligomers with Diverse Skeletons and Extracellular Regulated Protein Kinases Inhibitory Activity from *Sarcandra glabra*

Danyang Zhang, Zhiqi Xiao, An Huang, Pengfei Tang, Houli Jiang, Mengmeng Yu, Ze Zheng, Lingyi Kong,* and Jun Luo*



Cite This: *J. Nat. Prod.* 2025, 88, 2181–2192



Read Online

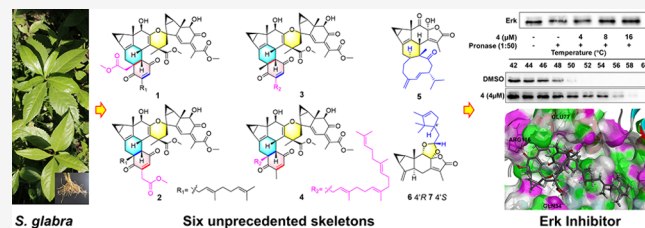
ACCESS |

Metrics & More

Article Recommendations

Supporting Information

ABSTRACT: Sarcglabtenes A–G (1–7), seven lindenane-based sesquiterpenoid hetero-oligomers with six unprecedented skeletons, along with five new biosynthetic analogues sarcglabtenes H–L (8–12), were isolated from *Sarcandra glabra*. Their structures including absolute configurations were comprehensively elucidated using HR-MS, NMR, ECD, and single crystal X-ray diffraction. Structurally, sarcglabtenes A–G are lindenane hetero-oligomers including a geranyl homogentisic acid (1/2), geranylgeranyl *p*-toluquinone (3/4), germarane (5), campholenal (6/7) derivatives, for which plausible biosynthesis pathways are also proposed. In bioassays, 1–4 exhibited cytotoxic activity against five cancer cell lines, and in particular, 4 acted as extracellular-regulated protein kinase (Erk) inhibitor of the MAPK signaling pathway involved in apoptosis.



Natural products have always played an irreplaceable and important role in the history of drug development.^{1,2} Their unique scaffolds and biological activities provide valuable molecular templates for the discovery of innovative drugs.^{1,2} Lindenane sesquiterpenoids (LSs), especially their oligomers, are the primary and characteristic metabolites of the Chloranthaceaeous plant, and exhibit a wide range of bioactivities, such as anti-inflammatory, antitumor, and antimalarial effects.³ The highly conjugated double bonds in LSs enable the formation of homo-oligomers via [4 + 2] cycloaddition, [2 + 2] cycloaddition, and [6 + 6] cycloaddition.³ Among the LS oligomers, the first to be discovered and the most common is the classical [4 + 2] dimer formed by the intermolecular Diels–Alder reaction between $\Delta^{15(4),5(6)}$ and $\Delta^{8,(9)}$.^{3–5} Furthermore, the lindenane unit of $\Delta^{15(4),5(6)}$ presents the capacity to engage with other double bonds found within the non-LS unit, thereby facilitating the formation of hetero-oligomers characterized by unparalleled structural diversity.^{6,7} Recently, an increasing number of such hetero-oligomers have been identified, including the LS and monoterpene dimers sarglaoxolanes A–C with anti-inflammatory activity, as well as the LS and *p*-benzoquinone-meroterpenoid trimer holotrichone B, known for its anti-leukemic properties.^{8,9} Given their exceptional structural variability, heteropolymerized lindenane oligomers, as a newly recognized class, exhibit significant potential for innovative biological activities and applications, deserving further investigation and exploration.

Encouraged by our previous research on LS from *S. glabra*,^{4,8} a well-known and commonly used traditional Chinese medicine, we conducted a reinvestigation of *S. glabra* to identify novel structures.^{10,11} As a result, sarcglabtenes A–G (1–7), seven lindenane-based sesquiterpenoid hetero-oligomers with six unprecedented skeletons and five new biosynthetic analogues (8–12), were discovered and comprehensively elucidated using HR-MS, NMR, ECD, and single crystal X-ray diffraction (Figure 1). Their cytotoxic activities against five cancer cell lines and the mechanism of action of the unique heterotrimer 4 as an extracellular regulated protein kinase (Erk) inhibitor were also elucidated. Herein, we report the isolation, structural elucidation, plausible biogenetic pathways, and Erk-targeted cytotoxicity of 1–12.

RESULTS AND DISCUSSION

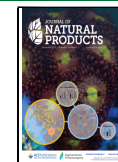
Sarcglabtene A (1) was obtained as a yellowish gum, and its molecular formula $C_{51}H_{60}NaO_{12}$ was established by the sodium adduct positive HRESIMS at m/z 887.3976 [$M + Na$]⁺ (calcd 887.3977), indicating the presence of 22 indices of hydrogen deficiency. The ¹H NMR (Table S1) and HSQC

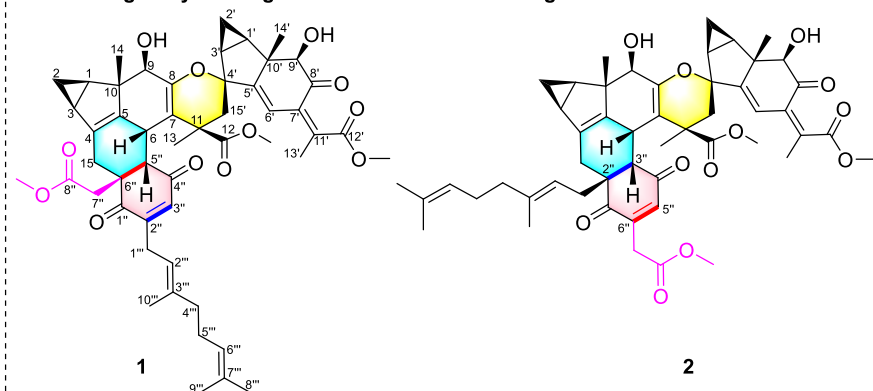
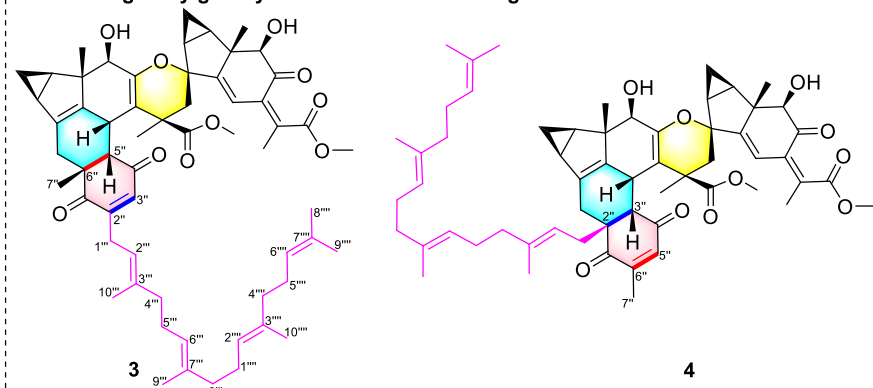
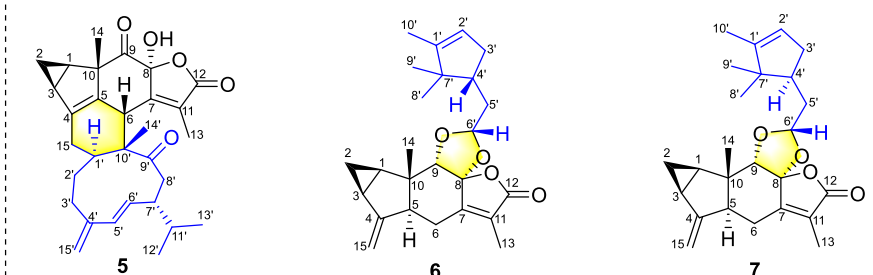
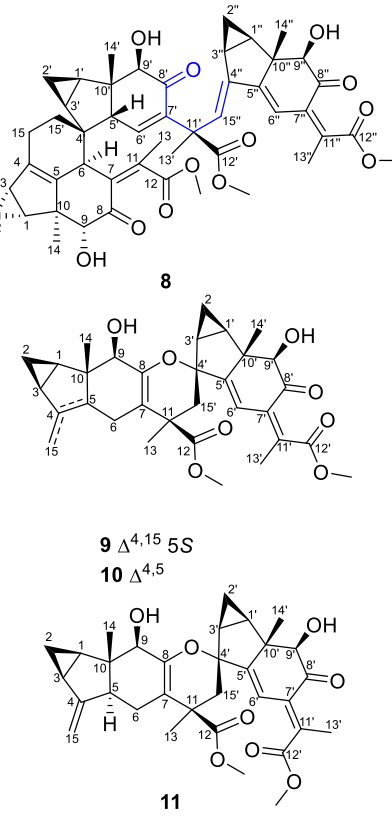
Received: June 25, 2025

Revised: July 29, 2025

Accepted: August 19, 2025

Published: September 1, 2025



Hetero-oligomers with novel skeletons**Lindenane-geranyl homogentisic acid Diels–Alder oligomers****Lindenane-geranylgeranyl toluene Diels–Alder oligomers****Lindenane-germarane/campholenal dimers****Homo-oligomers****Figure 1.** Chemical structures of sarcglabtenes A–L (1–12).

spectra showed two pairs of specific upfield characteristic cyclopropane methylene protons at δ_H 0.83 ($H-2\alpha$, overlapped)/0.18 ($H-2\beta$, m) and 0.77 ($H-2'\alpha$, m)/0.44 ($H-2'\beta$, m), characteristic geranyl protons at δ_H 5.12 ($H-2''$, br t 7.2) and 5.08 ($H-6''$, br t 7.2), and ten methyl protons at δ_H 0.86 (s), 1.17 (s), 1.30 (s), 1.60 (s), 1.62 (s), 1.68 (s), 2.14 (s), 3.67 (s), 3.68 (s) and 3.84 (s). The combination of δ_H 4.41 [$H-5'$, d (4.6)] with δ_C 200.6 ($C-1''$), and δ_C 199.3 ($C-4''$) revealed the existence of a quinone moiety. Thorough analysis of the NMR resonance spectra and MS data indicated that **1** was a novel hetero-LS oligomer consisting of two LS units and one other unit contained a quinone and a geranyl group.

The 1D NMR data of **1** were similar to those of holotrichone B with a $C_1-C_6-C_{10}$ unit C⁹; however, **1** featured a $C_2-C_6-C_{10}$ unit C, which was an essential difference in the skeleton. Unit C of **1** featured the substitution of a methyl acetate fragment for the methyl group at $C-6''$ in holotrichone B, and the replacement of the $\Delta^{2'',3''}$ double bond with the $\Delta^{5'',6''}$ double bond present on holotrichone B, both of which

were confirmed by key HMBC correlations (Figure 2A) from $H-7''$ to $C-1''$, $C-5''$ (δ_C 51.3), $C-6''$ (δ_C 52.1) and $C-8''$, from OCH_3-8'' to $C-8''$ and from $H-3''$ (δ_H 6.36, s) to $C-2''$ (δ_C 148.3). Furthermore, the $^1H-^1H$ COSY correlation between the proton signal of $H-6$ of unit A and $H-5''$ of unit C and the HMBC correlations (red arrows in Figure 2A) from proton signals of $H-5''$ of unit C to the carbon signals of unit A at $C-5$, $C-6$, $C-7$, and $C-15$, and from proton signals H_{2-15} of unit A to the carbon signals of unit C at $C-1''$, $C-5''$, $C-6''$, and $C-7''$, indicated that units A and C of **1** were bridged by the $C-15-C-6''$ and $C-6-C-5''$ bonds formed through [4 + 2] cycloaddition. Thus, the planar structure of **1** was thus delineated as the first example of a lindenane-geranyl homogentisic acid oligomer.

The relative configurations of units A and B were similar to that of holotrichone B,⁹ which was determined by ROESY correlations (Figure 2A) of $H-6/H-5''/H_3-13/H-15\alpha/H-6'$, and $H_3-13/H-15\beta/H-2\beta/H-3-14'$, as well as by biosynthetic considerations. H_3-13 exhibited a ROESY correlation with $H-$

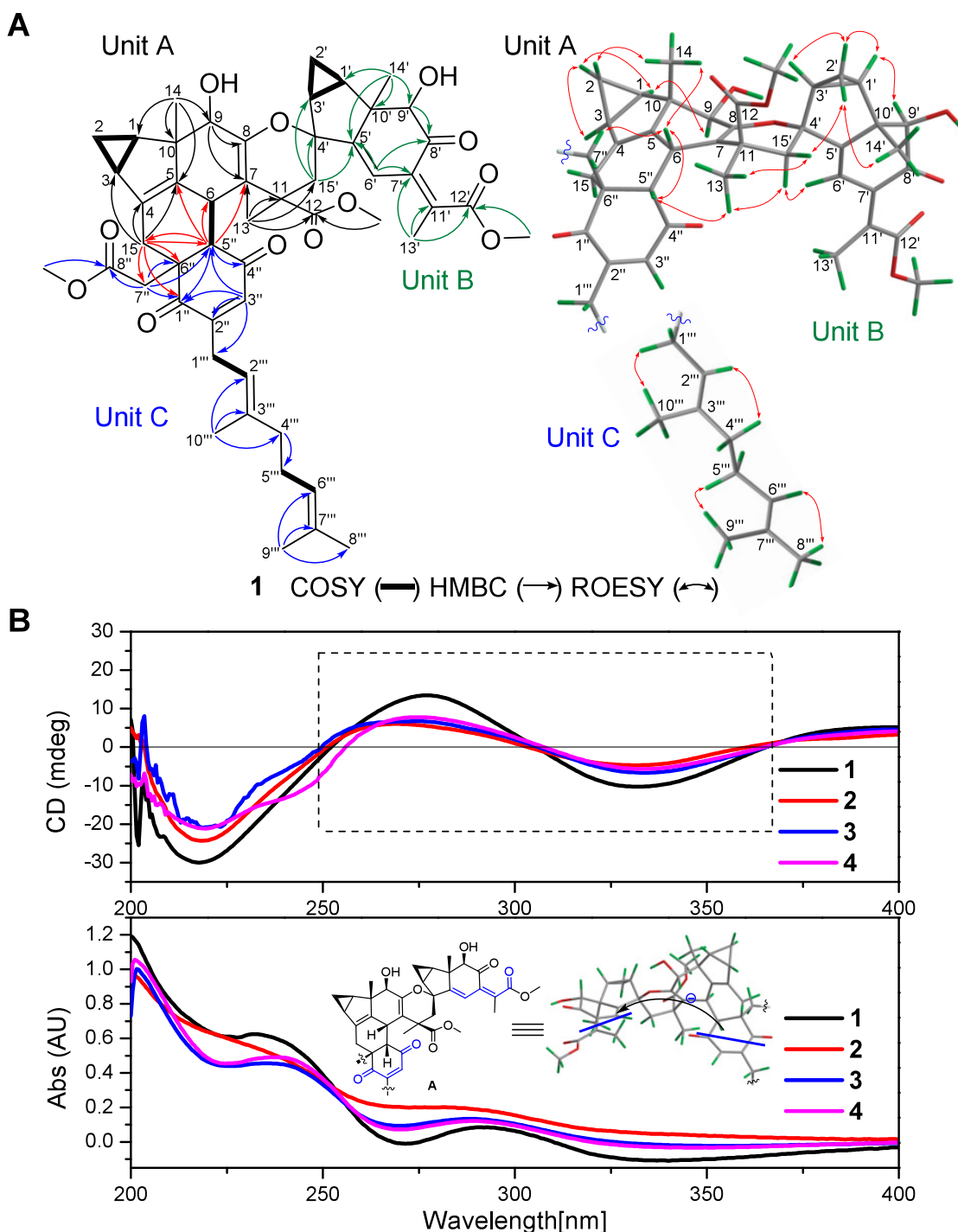


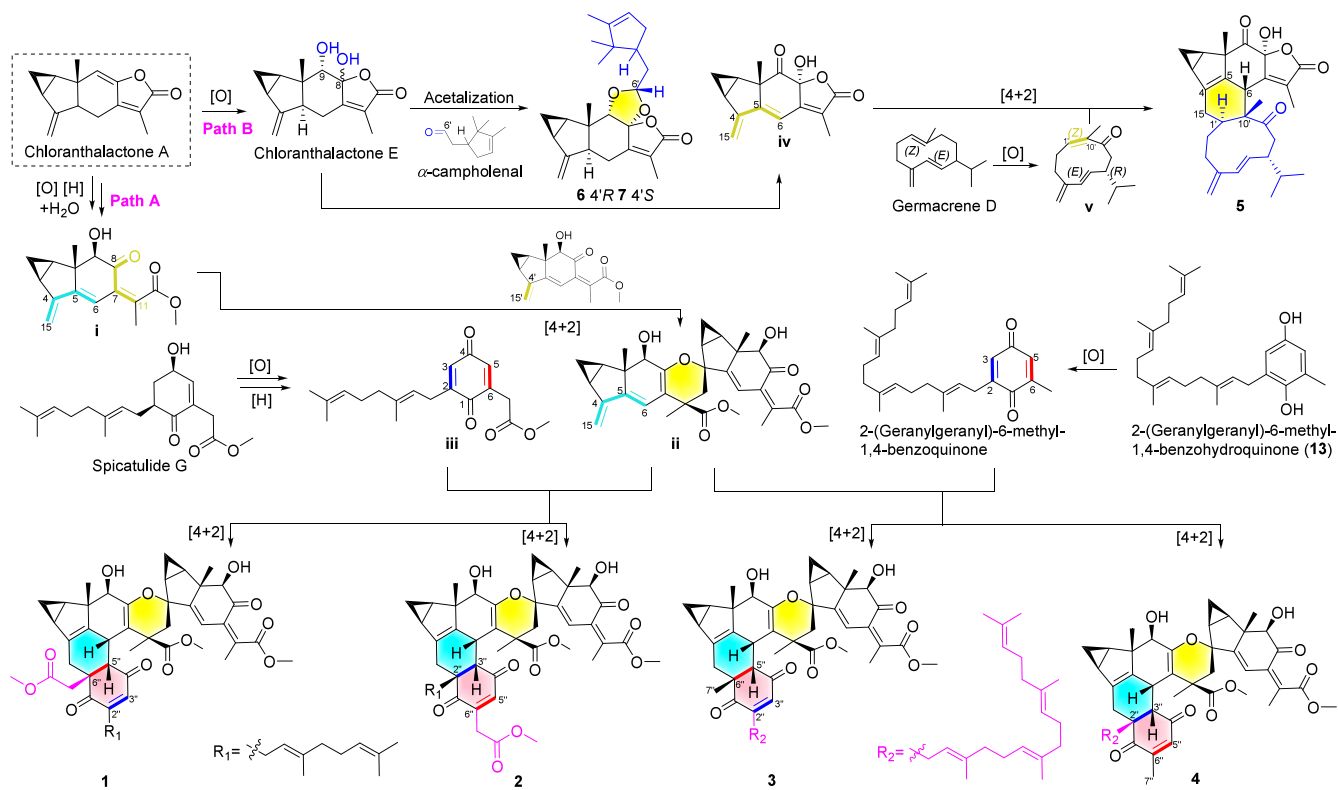
Figure 2. Structural elucidation of **1**. (A) Key 2D correlations of **1**, (B) experimental ECD and UV spectra of **1–4**.

⁵" on the α -configured C-5, which confirmed that H₃-13 was in the α -configuration (equatorial bond). The $\Delta^{2\pi/3, (3\pi)}$ and $\Delta^{6\pi/7, (7\pi)}$ double bonds were assigned an E-geometry by the ROESY correlations of H-1'''/H-10'', H-2'''/H-4'', H-5'''/H-9'', H-6'''/H-8''. The relative configuration at the new polymerization site in units A and C was established through key ROESY correlations of H-5''/H-6/H-7'' and H-6/H₃-14, indicating β -orientation of H-6, C-7'', and H-5''. The subsequently recorded ECD spectrum of **1** (Figure 2B) exhibited a split Cotton effect: a negative Cotton effect at 333 nm ($\Delta\epsilon - 1.57$) and a positive Cotton effect at 276 nm ($\Delta\epsilon + 2.00$), indicating a negative chirality that corresponded

to a counterclockwise transition-dipole arrangement between the two chromophores.¹² Furthermore, the experimental ECD trend of **1** was highly consistent with the experimental ECD trend of holotrichone B,⁹ whereas the absolute configurations of known LSs with overlapping biogenetic pathways further confirmed the above results.^{3, 9, 12b} Thus, the absolute configuration of **1** was established as 1*R*, 3*S*, 6*R*, 9*R*, 10*S*, 1' *R*, 3' *S*, 4' *R*, 9' *R*, 10' *S*, 5" *S*, 6" *S*.

Sarcoglbtene B (**2**) exhibited the same chemical formula ($C_{51}H_{60}NaO_{12}$) and similar 1D NMR data (Tables S1 and S2) as those of **1**, indicating the same biosynthetic precursors and polymerization form, the LS dimer (units A and B) and a

Scheme 1. Putative Biosynthetic Pathways for 1–7



geranyl homogentisic acid derivative (unit C). The difference lay in the fact that 2 was formed through the connection of two new bonds, C-15–C-2'' and C-6–C-3'', via a [4 + 2] cycloaddition pathway at new sites between units A and C, leading to the formation of a unique skeleton. This was further supported by the HMBC correlations from H₂-15 to C-1'', C-1'', C-2'' and C-3'', from H-3'' to C-5, C-6, C-7 and C-15 and the ¹H–¹H COSY correlation of H-6/H-3''. The similar ROESY data (Figure S1) and ECD spectrum (Figure 2B) of 2 and 1 suggested that these two compounds possessed identical relative and absolute configurations. Thus, the structure of 2 with new [4 + 2] polymerization framework was determined as shown in Figure 1.

Sarcglabtene C (3) and D (4) also showed same molecular formula C₅₉H₇₄O₁₀ based on ion peaks at *m/z* 965.5176 [M + Na]⁺ and 965.5177 [M + Na]⁺ in HRESI(+)MS spectra and similar 1D NMR data (Table S3 and Table S4), which indicated that they were also isomers as 1 and 2. By comparing their NMR data, 3 (Table S3) was structurally similar to 1 but differed in that 3 featured a new C₁–C₆–C₂₀ unit C instead of the C₂–C₆–C₁₀ unit C in 1. Unit C of 3 involved the substitution of a methyl group for the methyl acetate fragment at C-6'' in 1, and the replacement of the geranyl group at C-2'' with a geranylgeranyl group in 1, both of which were confirmed by key HMBC correlations (Figure S2) from H₂-15 to C-1'', C-5'', C-6'' and C-7'', from H-8''' to C-1''', from H₃-10''' to C-2''', C-3''', and C-4''', from H₂-4''' to C-5''', and from H₃-9''' to C-6''', C-7''', and C-8''', and the ¹H–¹H COSY correlation of H-2'''/H₂-1''', and H-6'''/H₂-5'''. Similar to 1, units A and C of 3 were unprecedentedly bridged by the C-15–C-6'' and C-6–C-5''' bonds through [4 + 2] cycloaddition, as evidenced by HMBC correlations from H₂-15 to C-1'', C-5'', C-6'', and C-7'', and from H-5''' to C-5'''.

C-6, C-7, and C-15, as well as ¹H–¹H COSY correlation of H-6/H-5''. The ¹H and ¹³C NMR spectra of 4 (Table S4) were very close to those of 3 (Table S3), with only difference on the chemical shifts for C-2'', C-3'', C-5'', C-6'', C-7'', and C-1''' of unit C. From a biosynthetic viewpoint, 3 might be biosynthesized from LS dimer (units A and B), which was supposed to be the diene, coupled with a dienophile group of the geranylgeranyl toluquinone (unit C) through a [4 + 2] cycloaddition (Scheme 1). Therefore, it was reasonable to infer that 4 was also formed from the same biosynthetic precursors of LS dimer (units A and B) and geranylgeranyl toluquinone (unit C) in another [4 + 2] cycloaddition direction, theoretically, based on the 1D NMR data between 3 and 4. This was secured by the key HMBC correlation of 4 (Figure S3) from H₂-15 to C-1'', C-2'', C-3'', and C-1''', and from H-3''' to C-5, C-6, C-7, and C-15, as well as ¹H–¹H COSY correlation of H-6/H-3''. The similar ROESY data of 3, 4 and 1 (Figure S2, Figure S3 and Figure 2A) suggested that they possessed similar relative configurations, with the *E*-geometry of the additional $\Delta^{2'''},(3'')}$ and $\Delta^{6'''},(7'')}$ double bonds in 3 and 4 being confirmed through analysis of the ROESY interaction (Figure S2 and Figure S3) between H-6'''/H-8''', H-5'''/H-9''', H-2'''/H-4''' and H-1'''/H-10'''. Similar to 1, the chiral centers of 3 and 4 were also located on the common parent nucleus A (Figure 2B) and ECD trends proved that 3, 4 and 1 have consistent absolute configurations. Thus, the structure of 3 and 4 were elucidated, marking the inaugural instance of an oligomeric of lindenane-C₁–C₆–C₂₀ geranylgeranyl toluquinone.

Sarcglabtene E (5) was obtained as a colorless crystal, with a molecular formula of C₃₀H₃₆O₅, determined by HRESIMS (*m/z* 499.2455 [M + Na]⁺). The ¹H NMR and HSQC spectra showed typical cyclopropane methylenes [δ_H 1.02 (m)/0.10

(m)] of the LS unit A (Table S5). Further HMBC correlations (Figure 3A) from H₂-15 to C-4 (δ_{C} 146.5) and C-5 (δ_{C} 125.0),

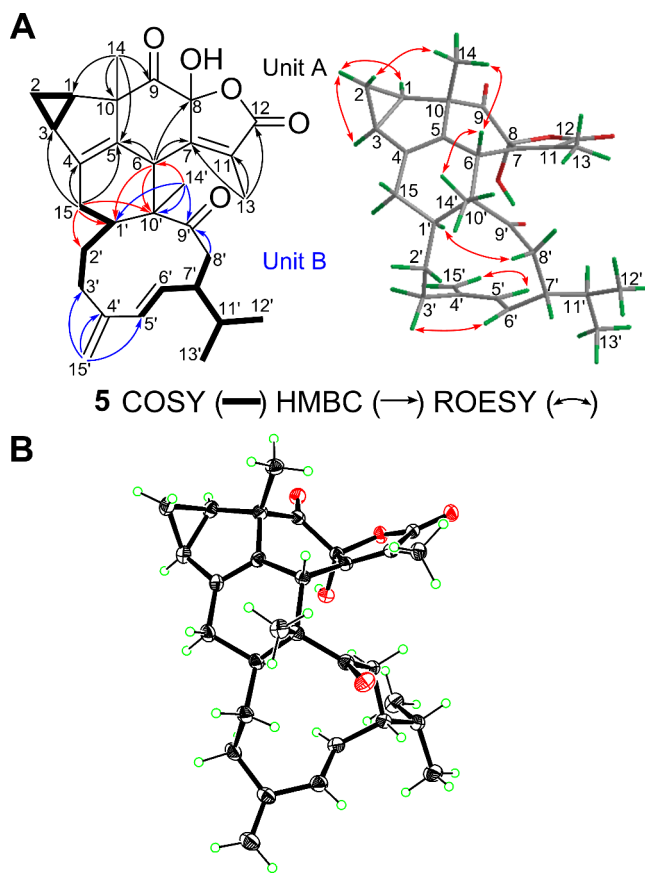


Figure 3. Structural elucidation of **5**. (A) Key 2D correlations and (B) X-ray crystallographic structure of **5**.

and from H-6 (δ_{H} 3.03, d 3.0) to C-5 showed that the LS unit A in **5** closely resembled unit A of chloranholide R,¹³ with $\Delta^{5,6}$ double bond replaced by $\Delta^{4,5}$ double bond and C-4 hydroxyl by CH-6. The remaining 15-carbons unit B contained an *E*-form (δ_{H} 5.81, d 16.2; δ_{H} 5.38, dd 16.2, 9.6) and terminal double bond (δ_{H} 4.79, br s; δ_{H} 4.74, br s), three methyl groups (δ_{H} 0.84, d 6.6; δ_{H} 0.81, d 6.6; δ_{H} 1.12, s), along with one keto carbonyl group (δ_{C} 214.0). And, the key HMBC correlations from H₂-15' to C-3', C-4' and C-5', from H-8' to C-9' and from H₃-14' to C-1', C-9' (δ_{C} 214.0) and C-10' along with ¹H-¹H COSY correlations of H-1'/H₂-2'/H₂-3', H-5'/H-6'/H-7'/H₂-8' and H-11'/H-7', H₃-12' and H₃-13' revealed that the unit B resembled those of the germacrene D,¹⁴ with the distinction being the presence of a C-9' ketone group and the disappeared $\Delta^{1',10'}$. Moreover, the ¹H-¹H COSY correlation of H₂-15/H-1' and the HMBC correlations from H₃-14' to C-6, from H-6 to C-10' and C-1' and from H₂-15 to C-1', C-2' and C-10' indicated that units A and B were bridged by a multiply substituted cyclohexene ring. The planar structure of **5** was thus delineated as an unprecedented lindenane and germarane sesquiterpenoid dimer. ROESY correlations (Figure 3A) of H-1/H-2 α /H-3, H₃-14'/H-6/H₃-14/H-2 β and H-1'/H-8' α indicated that H-2 β , H-6, H₃-14 and H₃-14' were β -oriented, while H-1, H-2 α , H-3 and H-1' was α -oriented. Finally, The X-ray diffraction data [Cu K α radiation, Flack parameter 0.010(15), CCDC 2435061] of **5**¹⁵ (Figure 3B) not only unambiguously determined its absolute configuration as

1R, 3S, 6S, 8S, 10S, 1'S, 7'R, 10'R, but also confirmed the skeleton as the first example of a lindenane-germacrene dimer.

Sarcglabtenes F (6) and G (7) had the same molecular formula, C₂₅H₃₂O₄ (10 degrees of unsaturation), as determined by HRESIMS and ¹³C NMR data. Analysis of their highly similar 1D NMR data revealed that **6** and **7** had the same planar structure. Their ¹H NMR spectrum only shown a set of characteristic cyclopropane methylene signals [δ_{H} 0.83 (m) and δ_{H} 0.67 (m)] of LSs (Table S6), and the remaining ten carbons indicated that they were LS-monoterpenoid dimer.¹⁶ Comparison of the 1D NMR (Table S6) between **6**, **7** and sarglalactone D indicated that the LS unit in **6** and **7** are identical to unit A of sarglalactone D.¹⁷ This was also confirmed by the key HMBC correlations (Figure 4A) from

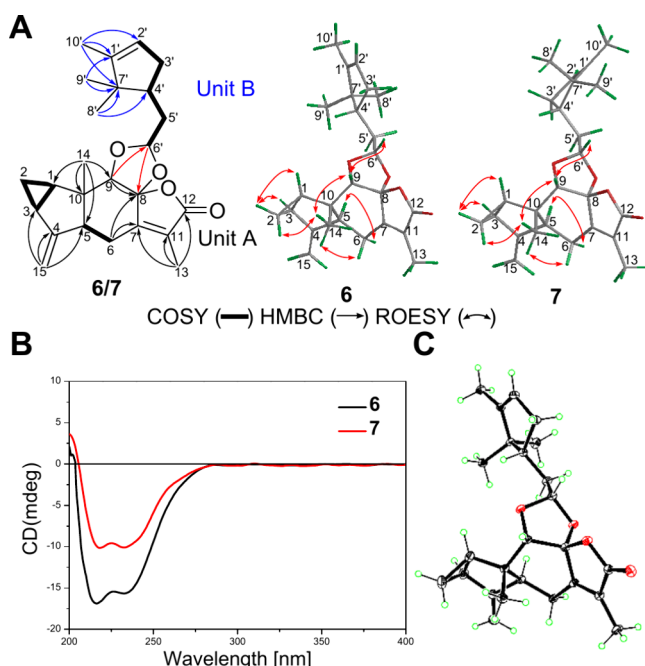


Figure 4. Structural elucidation of **6** and **7**. (A) Key 2D correlations of **6** and **7**, (B) experimental ECD spectra of **6** and **7**, and (C) X-ray crystallographic structure of **6**.

H₃-14 to C-1, C-5, C-9, and C-10, from H₂-15 to C-3, C-4 and C-5, from H₃-13 to C-7, C-11 and C-12, from H₂-6 to C-7 and C-8, and from H-9 to C-8, as well as ¹H-¹H COSY correlations of H-1/H₂-2/H-3 and H-5/H₂-6. HMBC correlations from H-8' to C-4' and C-7', from H-9' to C-1' and C-7', from H-10' to C-1', C-4' and C-7', as well as ¹H-¹H COSY correlations of H-2'/H₂-3'/H-4'/H₂-5'/H-6' (Figure 4A) indicated α -campholenal as the monoterpene unit.^{18,19} Moreover, the key HMBC correlations from H-6' of monoterpene unit B to C-8 (**6**, δ_{C} 109.9; **7**, δ_{C} 109.7) and from H-9 (**6**, δ_{H} 4.26, s; **7**, δ_{H} 4.28, s) of LS unit A to C-6' (**6**, δ_{C} 105.8; **7**, δ_{C} 106.0) indicated that sesquiterpenoid and monoterpene units were fused by a unique 1,3 dioxolane ring through acetalization, similar to sarglalactone D.¹⁷

The relative configuration of **6** and **7** was readily established using ROESY data (Figure 4A). ROESY correlations among **6**, **7** and sarglalactone D were similar, confirming that the relative configuration of unit A in **6** and **7** was consistent with that of sarglalactone D. The key to determining their relative configuration lay in H-6' and H-4' of the new polymerization unit B. The relative configuration of H-6' of **6** and **7** was

elucidated by ROESY correlations of H₃-14/H-9/H-6', which indicated that H-6' was β -oriented. However, the stereochemistry at the relative configurations of H-4' cannot be assigned due to the lack of definitive ROESY correlations. Further analysis of the above relative configurations, similar CD spectra (Figure 4B), along with slight NMR differences around the monoterpene unit of **6** and **7**, indicated they were C-4' isomers, thus the next task was to determine the relative configuration of C-4'. After testing various solvents and crystallization conditions, single crystals of **6** were obtained in a methanol-H₂O mixture at 4 °C. X-ray crystallography results (Figure 4C) not only determined the relative configuration at C-4' of **6** as shown in Figure 1, but also established the absolute configuration of **6** as 1R, 3S, 5S, 8S, 9S, 10S, 4'R, 5'S (Cu K α radiation, Flack parameter 0.01(4), CCDC 2435062).¹⁵ As a C-4' isomer of **6**, the absolute configuration of **7** was determined to be 1R, 3S, 5S, 8S, 9S, 10S, 4'S, 5'S. Therefore, the absolute configuration of **6** and **7**, representing the first examples of a lindenane-campholenal dimer, were established.

Sarcglabtene H (**8**) had the same molecular formula, C₄₈H₅₄O₁₂, as spirolindemer B,²⁰ as determined by the (+)-HRESIMS ion at *m/z* 845.3508 [M + Na]⁺ (calcd for C₄₈H₅₄O₁₂Na, 845.3507). The 1D NMR spectrum (Table S7) of **8** was similar to that of spirolindemer A, except for the absence of the $\Delta^{5'(6')}$ double bond and the 3,4-dihydro-2H-pyran ring in spirolindemer A and the presence of a $\Delta^{6'(7')}$ double bond, an *E*-configured $\Delta^{15'',(4'')}$ double bond, β -H and a C-8' keto-carbonyl group in **8**. This difference was confirmed by the ¹H-¹H COSY correlations (Figure 5A) of H-5' [δ_H]

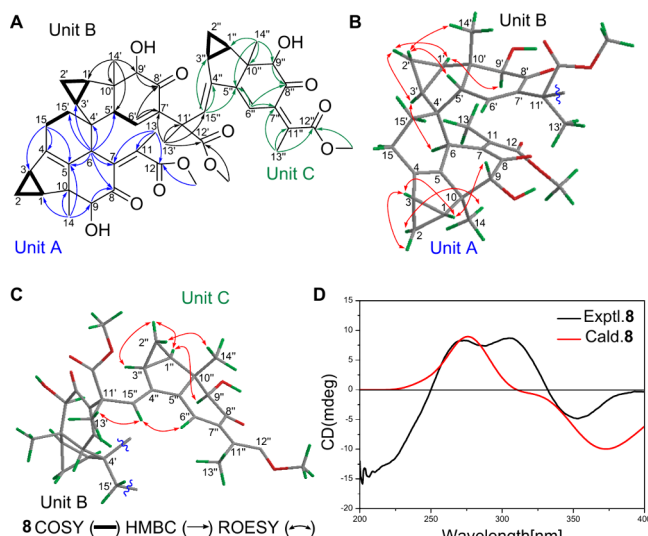


Figure 5. Structural elucidation of **8**. (A–C) Key 2D correlations of **8** and (D) experimental and calculated ECD spectra of **8**.

2.13, d (6.0)]/H-6' [δ_H 6.39, d (6.0)], the HMBC correlations from H-6' to C-7' (δ_C 138.5) and C-8' (δ_C 198.3) and from H-15'' [δ_H 5.59, s] to C-4'' (δ_C 143.8), along with the ROESY correlations (Figure 5B and 5C) of H-15''/H-6'' and H-5'/H-2' β . The absolute configuration of **8** was determined based on comparative analysis of calculated and experimental ECD curves (Figure 5D) as well as biogenic synthesis pathways.^{3,9,12} Thus, the structure of **8**, which represented the first LS trimer with an opened 3,4-dihydro-2H-pyran ring, was determined.

Sarcglabtenes I (**9**), J (**10**) and K (**11**) shared the same molecular formula (C₃₂H₃₈O₈Na), as revealed by the HRESIMS, which was 2 mass units more than that of spirolindemer A.²⁰ Comparison of 1D NMR data of **9** (Table S8) with those of spirolindemer A indicated the replacement of the C-9 carbonyl group in spirolindemer A by a C-9 hydroxy group in **9**, as supported by the key HMBC correlation (Figure 6A) from CH₃-14 to C-9 (δ_C 76.4). The ROESY correlation (Figure 6A) of H-1/H-9 indicated that the relative configuration of the C-9 hydroxy group was β -oriented. The ECD curves of **9** were in good agreement with those of our previously reported spirolindemer A (Figure 6B).²⁰ Therefore, the absolute structures of **9** were defined. Analysis of NMR data of **10** and **11** (Table S9) revealed that their structures were closely related to that of **9**. Compared with **9**, the disappearance of the terminal double bond and the appearance of the CH₃-15 and $\Delta^{4,(5)}$ double bonds in **10** were confirmed by key HMBC correlations (Figure S4) from H₃-15 (δ_H 1.71, br s) to C-4 (δ_C 134.7) and C-5 (δ_C 132.5), while in compound **11**, the only difference was that the $\Delta^{7',(11')}$ double bond is in the *E* configuration, which is consistent with the previously reported relationship between henriol C and shizukaol B²¹ and was also confirmed by the downfield shifts of the proton signals at δ_H 6.71 (s, H-6') and 2.40 (s, H₃-13') compared with the corresponding proton resonances of **9** [δ_H 6.39 (s, H-6'), 2.09 (s, H₃-13')], as well as the differences in the chemical shifts of C-11' (δ_C 137.5) and C-8' (δ_C 202.3) compared with those of **9** [δ_C 138.2 (C-11') and δ_C 198.6 (C-8')]. The ROESY correlations (Figure S4 and S5) and ECD curves (Figure 6B) of **10** and **11** were in good agreement with those of **9** (Figure 6). Therefore, the absolute structures of **10** and **11** were defined.

Sarcglabtene L (**12**), a white, amorphous, purified powder, had the molecular formula C₃₀H₃₂O₈, based on its HRESIMS data. Its 1D NMR (Table S10) data showed similarities to those of our previously reported sarglactone D,¹⁷ except for a 1,3-dioxolane ring being replaced by an ester bond (C-9, δ_C 77.0; C-9', δ_C 176.8) and β -OH-8 (C-8, δ_C 105.1) in **12**. This conclusion was confirmed by the HMBC correlations (Figure 7A) from H-9 to C-8 and C-9'. Furthermore, according to reference,²² the α -orientation of C(8)-OH corresponded with the proton chemical shift of CH₃-14 in a range of 0.42–0.67 ppm, while a shift in the range of 0.82–1.47 ppm for CH₃-14 corresponded to the β -orientation of C(8)-OH. Thus, the proton chemical shift of CH₃-14 (δ_H 1.03, s) in **12** indicated that the C(8)-OH was β -orientation. The absolute configuration of **12** was assigned by applying the exciton chirality CD method (Figure 7B) and known LSs with similar biogenetic pathways.^{3,9,12}

The novel polymeric units and rare polymerization forms of hetero-oligomers **1**–**7** prompted us to summarize their plausible biosynthetic pathways (Scheme 1). According to their structures, chloranthalactone A was considered as the precursor of lindenane unit,^{8,23} which underwent oxidation, reduction, and lactonization to form diverse derivatives as intermediates for subsequent transformations with other non-LS units.²⁴ In path A, an oxygenated [4 + 2] cycloaddition at nonclassical positions, with the $\Delta^{7(11),8(O)}$ of **i** acting as the diene moiety and the $\Delta^{15'',(4'')}$ of another **i** acting as the dienophile moiety, produced **ii**, which was equipped with the same oxaspido[4.5]decane as previously reported spirolindemer A.²⁰ Spicatulide G underwent redox reactions to form intermediate **iii**.²⁵ The coisolated **13** was oxidized to generate

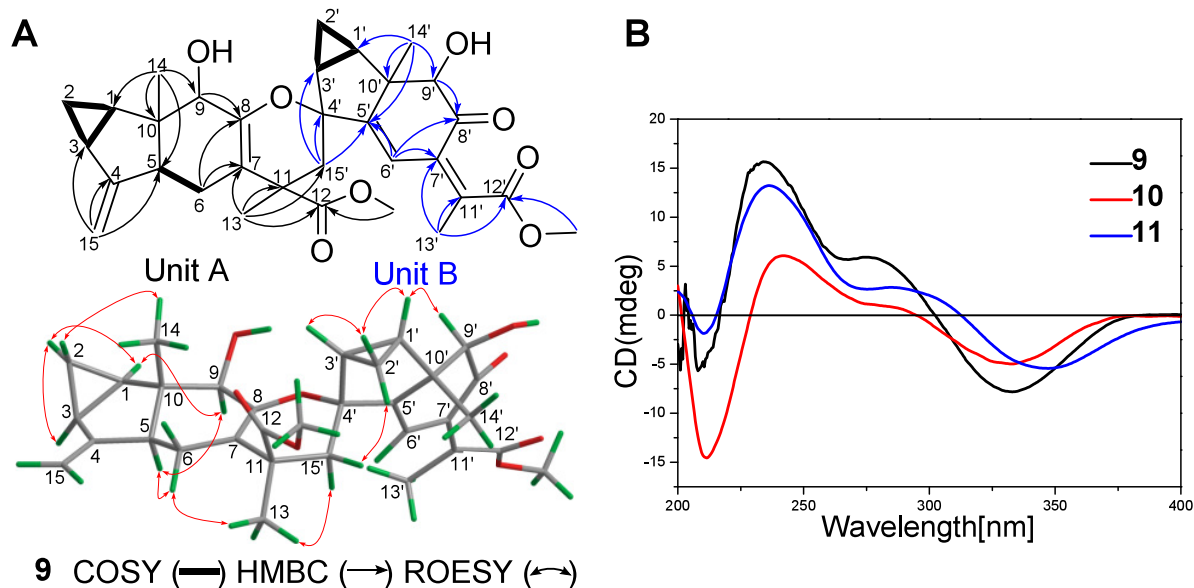


Figure 6. Structural elucidation of 9. (A) Key 2D correlations of 9 and (B) experimental ECD spectra of 9–11.

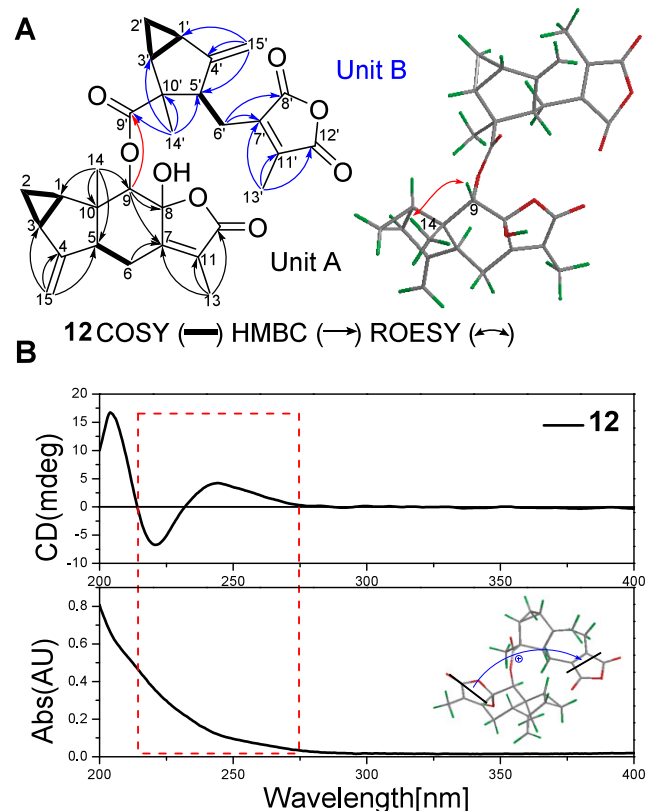


Figure 7. Structural elucidation of 12. (A) Key 2D correlations of 2 and (B) experimental ECD and UV spectra of 12.

intermediate 2-(Geranylgeranyl)-6-methyl-1,4-benzoquinone.²⁶ Intermediate ii with $\Delta^{15(4),5(6)}$ diene moieties reacted with iii containing two $\Delta^{5(6)}$ and $\Delta^{2(3)}$ dienophile moieties via [4 + 2] cycloaddition to produce 1 and 2, respectively.⁹ Similar to 1 and 2, intermediate ii and 2-(Geranylgeranyl)-6-methyl-1,4-benzoquinone underwent [4 + 2] cycloaddition to generate 3 and 4. In path B, chloranthalactone E reacted with α -campholenal^{18,19} via acetalization to produce 6 and 7 with a rare 1,3 dioxolane ring as sarglactone D.¹⁷ Intermediate iv

reacted with the oxidation product v of germacrene D¹⁴ through a [4 + 2] cycloaddition to yield 5 with a unique skeleton.

In recent years, the traditional herbal medicine *S. glabra* has been widely used to treat various cancer types, including pancreatic, gastric, rectal, liver, and esophageal cancer.^{10,27} This prompted an evaluation of the cytotoxic activities of sarcglabtenes A–L (1–12). As shown in Figure 8A, unique hetero-LS trimers 1–4 exhibited cytotoxic activity, with 4 showing an IC_{50} value of $4.06 \pm 0.11 \mu\text{M}$ against MDA-MB-231 cells, a highly metastatic breast cancer cell line, which was 3-fold more potent than the positive control DDP. Thus, 4 was selected for further investigation. Initially, we investigated whether 4 affected the epithelial-mesenchymal transition (EMT) process in these cells. Scratch assays showed that 4 could concentration-dependently downregulate the migratory capacity of MDA-MB-231 cells (Figure 8B). Western blotting analysis also confirmed that 4 inhibited the phosphorylation of JNK, Erk, MEK, and p38 proteins in the MAPK pathway (Figure 8C and Figure S7), while upregulating E-cadherin and downregulating the expression of N-cadherin and zonula occludens-1 (ZO-1) (Figure 8D and Figure S8). By inhibiting the phosphorylation and activation of the MAPK pathway, 4 disrupted the EMT process, thereby suppressing cell migration and invasion. Additionally, Annexin V/PI staining and flow cytometry analysis demonstrated that 4 significantly induced apoptosis (Figure 8E). Western blotting results also showed that 4 promoted the cleavage of caspase-dependent apoptotic proteins (caspase-3, caspase-9, PARP) and upregulated the expression of pro-apoptotic protein Bax while downregulating the antiapoptotic protein Bcl-2 (Figure 8F and Figure S9), thereby accelerating apoptosis in MDA-MB-231 cells. Drug affinity responsive target stability (DARTS) experiments indicated that 4 bound to proteins in the 40–50 kDa range (Figure S6). This molecular weight range includes the Erk protein that activates and regulates various transcription factors through phosphorylation in the MAPK pathway, promoting cell proliferation and protecting cells from apoptosis.²⁸ Using DARTS-Western blotting, we confirmed significant interaction between 4 and Erk protein (Figure 8G and Figure S10).

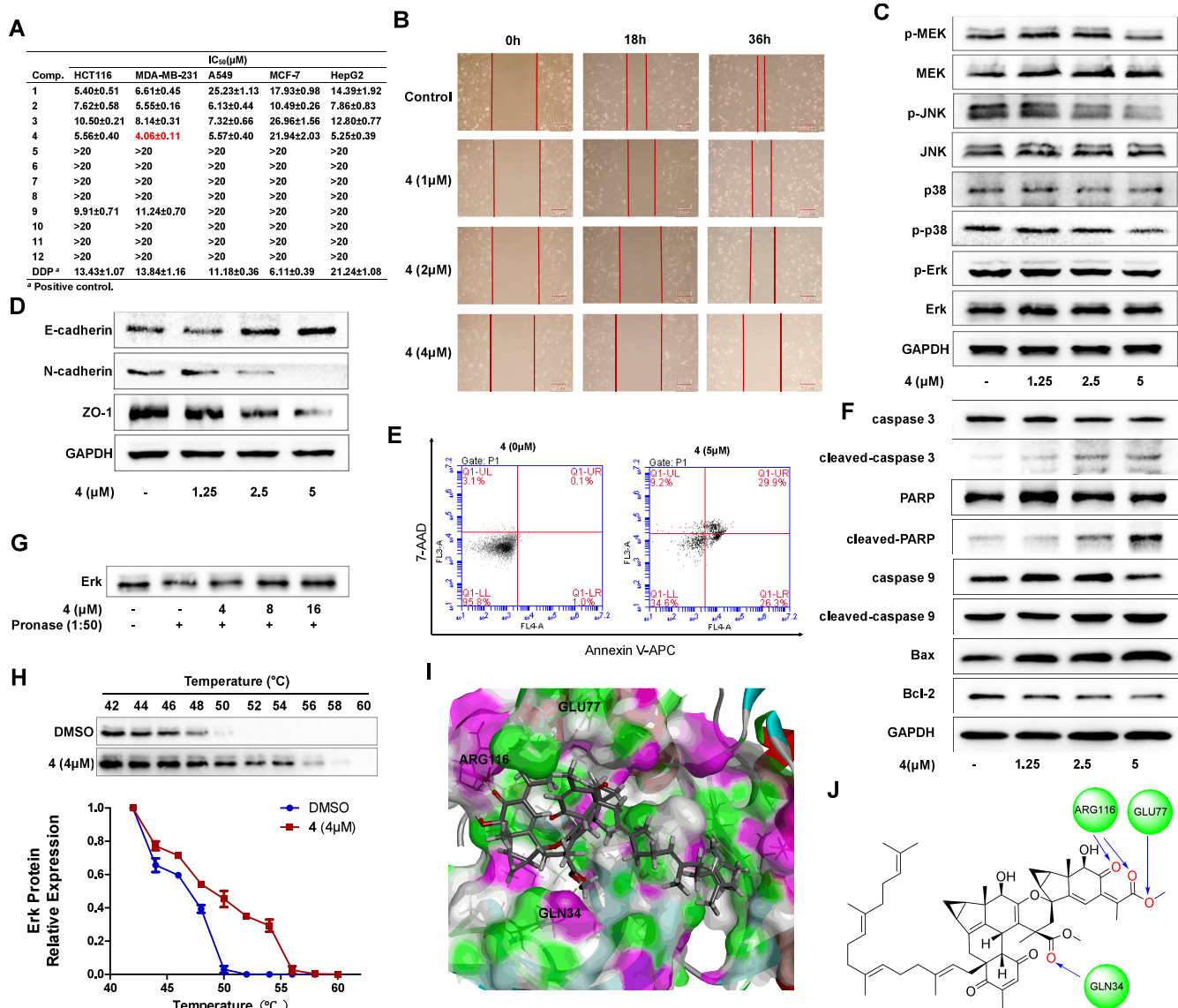


Figure 8. Compound 4 interacts with Erk to inhibit the MAPK pathway, disrupt EMT, reduce tumor cell migration and invasion, and induce apoptosis. (A) Calculation of IC₅₀ values for 1–12. (B) Cell scratch test was performed to measure the migration ability of 4 and MDA-MB-231 cells. (C) Expression levels of MAPK pathway-related proteins after 4 treatment. (D) Expression levels of EMT-related proteins after 4 treatment. (E) Flow cytometry analysis of the effect of 4 on MDA-MB-231 cell apoptosis. (F) Expression levels of apoptosis-related proteins after 4 treatment. (G) DARTS-Western blot experimental validation of the interbinding interaction of 4 with Erk proteins. (H) CETSA analysis of intracellular binding between 4 and Erk. Protein levels were investigated at different temperatures under the treatment of 4 (4 μM) in MDA-MB-231 cells. (I,J) Interactions based on molecular docking studies between Erk 1 protein (PDB: 4QTB) with 4.

Cellular thermal shift assay (CETSA) further validated that 4 enhanced the thermal stability of Erk protein, confirming their direct interaction (Figure 8H). Molecular docking results also supported this finding (Table S11, Figure 8I, Figure 8J, Figure S11 and Figure S12). In summary, 4 bound to Erk protein, inhibited the activation of the MAPK pathway, disrupted the EMT process, suppressed tumor cell migration and invasion, and induced apoptosis, thus providing promising evidence supporting its application as a lead compound for the development of novel Erk inhibitors.

In summary, sarcoglabetenes A–G (1–7), seven lindenane-based sesquiterpenoid hetero-oligomers with six unprecedented skeletons, along with five new biosynthetic analogues (8–12), were discovered from *S. glabra*, a famous and commonly used traditional Chinese Medicine. Structurally,

they represent the first examples of lindenane-based hetero-oligomers with geranyl homogenetic acid (1/2), geranylgeranyl *p*-toluquinone (3/4), germarane (5), campholenal (6/7) derivatives, greatly enriching the structural diversity of the LS scaffold. Considering the diversity of nonlindenane components in plants containing lindenane, additional LS hetero-oligomers remain to be discovered, which will provide new directions for the future development of LSs. Notably, these heterosesquiterpenoid oligomeric scaffolds derived from lindenane represent a unique class of natural compounds that target Erk, a critical protein kinase involved in cell signaling pathways. When dysregulated, Erk is intricately linked to cancer progression, making it an increasingly critical therapeutic target in oncology. Thus, the discovery of these compounds not only highlights the great potential of this

emerging group of lindenane-based oligomers but also provides a promising source for the development of new Erk inhibitors as anticancer lead compounds, serving as a rationale for further research and application of *S. glabra* as an anticancer drug.

■ EXPERIMENTAL SECTION

General Experimental Procedures. Melting points were measured using a RY-1G apparatus. Optical rotations were measured in methanol through a JASCO P-1020 polarimeter. The UV absorbance was determined on a Shimadzu UV-2450 UV-vis spectrophotometer. IR spectra were recorded on a Nicolet iS10 FT-IR and Bruker Tensor-27 infrared spectrophotometer. The JASCO J-810 spectrometer was used to record the ECD spectra (measured in methanol at 25 °C). NMR spectra were recorded on the Bruker AV-600 NMR instrument (Bruker, Karlsruhe, Germany) at 25 °C. TMS was used as the internal standard, and CDCl₃, MeOD or CD₃COOD as solvents. Structural assignments were completed through additional information from gCOSY, gHSQC, gHMBC, and ROESY experiments. HRESIMS data were acquired on an Agilent 6520B UPLC-Q-TOF instrument. Preparative HPLC was performed on the Shimadzu LC-20AR system with a UV detector (SPD-20A), which was equipped with an Ultimate XB-C18 column (250 mm × 20 mm i.d., 5 μm) with a flow rate of 10.0 mL/min. The samples were analyzed by HPLC using an Agilent 1100 system equipped with a DAD detector and an Agilent ZORBAX Eclipse XDBC18 column [5 μm, 150 × 4.6 mm (i.d.)] or a Phenomenex Cellulose-2 chiral column (5 μm, 250 × 4.6 mm), with a flow rate of 1 mL/min in either CH₃OH/H₂O or CH₃CN/H₂O solvent systems. Column chromatography (CC) separations were carried out using silica gel (100–200 mesh and 200–300 mesh; Qingdao Haiyang Chemical Co., Ltd., Qingdao, China), MCI (Mitsubishi, Japan), YMC-Gel RP-C18 (50 μm; YMC, Milford, MA), and Sephadex LH-20 (40–70 μm; Amersham Pharmacia Biotech AB, Uppsala, Sweden). The thin-layer chromatography (TLC) analysis was performed on precoated silica gel GF254 plates.

Plant Material. The roots of *Sarcandra glabra* (Thunb.) Makino were collected in Sanming (26° 15' N, 117° 27' E), Fujian Province, People's Republic of China, in August 2019. Identification of the plant samples was completed by Prof. Mian Zhang at China Pharmaceutical University. A voucher specimen (no. 20190802) was deposited at the Department of Natural Medicinal Chemistry at China Pharmaceutical University.

Extraction and Isolation. The powder of dried roots of *S. glabra* (20 kg) was extracted for three times with 95% EtOH under reflux (3 h, 2 h, 2 h). The filtrate was concentrated under vacuum to obtain the crude extract (960g), which was then suspended in water and partitioned with CH₂Cl₂. The CH₂Cl₂ extracts (330 g) were separated by silica gel column chromatography through gradient elution of CH₂Cl₂/CH₃OH (from 100:1 to 2:1) to yield eight major fractions (Fr.1–8). Fr.3 (17.5 g) was chromatographed over an MCI gel column (CH₃OH/H₂O from 50:50 to 100:0) to give ten fractions (Fr.3A–3J). Fr. 3C (2.5 g) was partitioned on a Sephadex LH-20 eluted with CH₃OH and purified by reversed-phase preparative HPLC using 70% MeOH to yield **6** (2 mg, 31 min) and **7** (1.5 mg, 33 min). Fr. 3I (1.9 g) was partitioned on a Sephadex LH-20 eluted with CH₂Cl₂/CH₃OH (1:1) and purified by reversed-phase preparative HPLC using 95% MeOH to yield **5** (3 mg, 24 min). Fr. 3H (1.2 g) was partitioned on a Sephadex LH-20 eluted with CH₂Cl₂/CH₃OH (1:1) and purified by reversed-phase preparative HPLC using 100% MeOH to yield **13** (40 mg, 13 min). Fr. 3J (2 g) was partitioned on a Sephadex LH-20 eluted with CH₂Cl₂/CH₃OH (1:1) and purified by reversed-phase preparative HPLC using 98% CH₃CN/H₂O to yield **4** (10 mg, 19 min) and **3** (30 mg, 22 min). Fr.4 (40 g) was chromatographed over an MCI gel column (CH₃OH/H₂O from 30:70 to 100:0) to give four fractions (Fr.4A–4D). Fr.4B (9 g) was chromatographed on an ODS column using CH₃OH/H₂O (50:50 to 100:0) to yield four fractions (Fr.4B1–4B4). Fr.4B3 (1.9 g) was separated over a Sephadex LH-20 gel (CH₃OH) to obtain eight

fractions (Fr.4B3A–Fr.4B3H). Fr.4B3F (207.2 mg) was chromatographed by HPLC with CH₃OH/H₂O (80:20) to yield **9** (30 mg, 48 min), **11** (5 mg, 50 min) and **10** (3 mg, 55 min). Fr.4B4 (2.0 g) was separated over a Sephadex LH-20 gel (CH₂Cl₂/CH₃OH = 1:1) to obtain seven fractions (Fr.4B4A–Fr.4B3G). Fr.4B4C (110.1 mg) was chromatographed by HPLC with CH₃OH/H₂O (85:15) to yield **12** (4 mg, 32 min). Fr.4D (8 g) was chromatographed on an ODS column using CH₃OH/H₂O (50:50 to 100:0) to yield four fractions (Fr.4D1–4D4). Fr.4D4 (2.7 g) was partitioned into nine subfractions (Fr. 4D4A – 4D4I) using Sephadex LH-20 eluted with CH₂Cl₂/CH₃OH (1:1). Fr. 4D4I (135.2 mg) was chromatographed by HPLC with CH₃CN/H₂O (80:20) to yield **2** (1.6 mg, 25 min) and **1** (2.5 mg, 30 min). Fr.5 (83.9 g) was chromatographed over an MCI gel column (CH₃OH/H₂O from 50:50 to 100:0) to give 12 fractions (Fr.5A–5L). Fr.5G (8.4 g) was chromatographed on an ODS column using CH₃OH/H₂O (50:50 to 100:0) to yield eight fractions (Fr.5G1–5G8). Fr.5G7 (2.4 g) was partitioned on a Sephadex LH-20 eluted with CH₂Cl₂/CH₃OH (1:1) and purified by reversed-phase preparative HPLC using CH₃CN/H₂O (55:45) to yield **8** (3 mg, 42 min).

Sarcglabtene A (1). yellowish gum; $[\alpha]_D^{25} = -65.1$ (*c* = 0.10 in MeOH); ¹H and ¹³C NMR data, see Table S1; IR: ν_{\max} = 3708, 2935, 2857, 1725, 1676, 1599, 1431, 1360, 1297, 1237, 1163, 1029, 996, 910, 728 cm⁻¹; UV (MeOH): λ_{\max} (log ϵ) = 235 (4.21), 293 (0.48) nm; CD (MeOH): λ (Δ ϵ) = 217 (-4.63), 276 (2.00), 333 (-1.57) nm; (+)-HRESIMS: *m/z* 887.3976 [M + Na]⁺ (calcd for C₅₁H₆₀O₁₂Na, 887.3977).

Sarcglabtene B (2). yellowish gum; $[\alpha]_D^{25} = -62.2$ (*c* = 0.10 in MeOH); ¹H and ¹³C NMR data, see Table S2; IR: ν_{\max} = 3472, 2932, 2866, 1728, 1679, 1638, 1594, 1438, 1378, 1301, 1227, 1116, 1095, 1033, 1005, 906, 728 cm⁻¹; UV (MeOH): λ_{\max} (log ϵ) = 225 (4.17), 288 (1.39) nm; CD (MeOH): λ (Δ ϵ) = 219 (-4.35), 273 (1.05), 333 (-0.88) nm; (+)-HRESIMS: *m/z* 887.3976 [M + Na]⁺ (calcd for C₅₁H₆₀O₁₂Na, 887.3977).

Sarcglabtene C (3). yellowish gum; $[\alpha]_D^{25} = -62.6$ (*c* = 0.10 in MeOH); ¹H and ¹³C NMR data, see Table S3; IR: ν_{\max} = 3467, 2922, 2848, 1725, 1683, 1602, 1432, 1373, 1304, 1226, 1164, 1095, 1037, 1002, 758 cm⁻¹; UV (MeOH): λ_{\max} (log ϵ) = 238 (4.06), 289 (0.92) nm; CD (MeOH): λ (Δ ϵ) = 219 (-4.76), 277 (1.77), 333 (-1.44) nm; (+)-HRESIMS: *m/z* 965.5176 [M + Na]⁺ (calcd for C₅₉H₇₄O₁₀Na, 965.5174).

Sarcglabtene D (4). yellowish gum; $[\alpha]_D^{25} = -60.4$ (*c* = 0.10 in MeOH); ¹H and ¹³C NMR data, see Table S4; IR: ν_{\max} = 3478, 2973, 2911, 2854, 1728, 1679, 1638, 1426, 1369, 1308, 1230, 1156, 1095, 1034, 1001, 952, 756 cm⁻¹; UV (MeOH): λ_{\max} (log ϵ) = 239 (4.07), 290 (0.93) nm; CD (MeOH): λ (Δ ϵ) = 219 (-4.77), 277 (1.76), 333 (-1.45) nm; (+)-HRESIMS: *m/z* 965.5177 [M + Na]⁺ (calcd for C₅₉H₇₄O₁₀Na, 965.5174).

Sarcglabtene E (5). colorless crystal; mp 237–237.5 °C; $[\alpha]_D^{25} = +58.4$ (*c* = 0.10 in MeOH); ¹H and ¹³C NMR data, see Table S5; IR: ν_{\max} = 3388, 2957, 2876, 1852, 1772, 1730, 1660, 1558, 1452, 1384, 1113, 963, 895 cm⁻¹; UV (MeOH): λ_{\max} (log ϵ) = 232 (1.53) nm; (+)-HRESIMS: *m/z* 499.2455 [M + Na]⁺ (calcd for C₃₀H₃₆O₅Na, 499.2455).

Sarcglabtene F (6). colorless crystal; mp 184–184.6 °C; $[\alpha]_D^{25} = +51.1$ (*c* = 0.10 in MeOH); ¹H and ¹³C NMR data, see Table S6; IR: ν_{\max} = 2962, 2918, 2849, 2821, 1777, 1645, 1413, 1153, 970, 933, 881, 753 cm⁻¹; UV (MeOH): λ_{\max} (log ϵ) = 217 (1.42) nm; CD (MeOH): λ (Δ ϵ) = 218 (-3.77), 234 (-3.73) nm; (+)-HRESIMS: *m/z* 419.2191 [M + Na]⁺ (calcd for C₂₅H₃₂O₄Na, 419.2193).

Sarcglabtene G (7). white amorphous solid; $[\alpha]_D^{25} = +54.3$ (*c* = 0.10 in MeOH); ¹H and ¹³C NMR data, see Table S6; IR: ν_{\max} = 2917, 2849, 1768, 1645, 1466, 1418, 1125, 966, 930, 644 cm⁻¹; UV (MeOH): λ_{\max} (log ϵ) = 218 (1.08) nm; CD (MeOH): λ (Δ ϵ) = 216 (-6.26), 234 (-5.80) nm; (+)-HRESIMS: *m/z* 419.2195 [M + Na]⁺ (calcd for C₂₅H₃₂O₄Na, 419.2193).

Sarcglabtene H (8). yellowish gum; $[\alpha]_D^{25} = +55.3$ (*c* = 0.10 in MeOH); ¹H and ¹³C NMR data, see Table S7; IR: ν_{\max} = 3487, 2948, 1726, 1682, 1592, 1433, 1376, 1229, 1082, 1032, 993, 806 cm⁻¹; UV (MeOH): λ_{\max} (log ϵ) = 213 (3.23), 255 (3.12), 306 (2.34) nm; CD

(MeOH): λ ($\Delta \epsilon$) = 220 (−6.27), 272 (4.20), 305 (4.36), 305 (−2.47) nm; (+)-HRESIMS: m/z 845.3508 [M + Na]⁺ (calcd for C₄₈H₅₄O₁₂Na, 845.3507).

Sarcglabtene I (9). white solid; $[\alpha]_D^{25} = -72.7$ ($c = 0.10$ in MeOH); ¹H and ¹³C NMR data, see Table S8; IR: $\nu_{\text{max}} = 3468, 2950, 2840, 1729, 1659, 1598, 1432, 1377, 1300, 1217, 1112, 1092, 1037, 1029, 991, 939, 876, 762, 630 \text{ cm}^{-1}$; UV (MeOH): λ_{max} (log ϵ) = 232 (4.11), 287 (2.59) nm; CD (MeOH): λ ($\Delta \epsilon$) = 234 (+7.23), 276 (+2.74), 333 (−3.55) nm; (+)-HRESIMS: m/z 573.2458 [M + Na]⁺ (calcd for C₅₉H₇₄O₁₀Na, 573.2459).

Sarcglabtene G (10). white solid; $[\alpha]_D^{25} = +78.1$ ($c = 0.10$ in MeOH); ¹H and ¹³C NMR data, see Table S9; IR: $\nu_{\text{max}} = 3468, 2954, 2928, 1729, 1436, 1378, 1300, 1227, 1150, 1099, 1033, 948, 765, 734 \text{ cm}^{-1}$; UV (MeOH): λ_{max} (log ϵ) = 219 (3.20), 287 (1.41) nm; CD (MeOH): λ ($\Delta \epsilon$) = 211 (−7.44), 242 (2.99), 332 (−2.56) nm; (+)-HRESIMS: m/z 573.2461 [M + Na]⁺ (calcd for C₃₂H₃₈O₈Na, 573.2459).

Sarcglabtene K (11). white solid; $[\alpha]_D^{25} = +64.1$ ($c = 0.10$ in MeOH); ¹H and ¹³C NMR data, see Table S9; IR: $\nu_{\text{max}} = 3456, 2976, 2953, 2920, 2867, 2847, 1726, 1661, 1434, 1373, 1214, 1159, 1057, 3481, 1012, 882, 772 \text{ cm}^{-1}$; UV (MeOH): λ_{max} (log ϵ) = 226 (3.55), 298 (1.99) nm; CD (MeOH): λ ($\Delta \epsilon$) = 211 (−1.08), 237 (6.65), 332 (−2.77) nm; (+)-HRESIMS: m/z 573.2461 [M + Na]⁺ (calcd for C₃₂H₃₈O₈Na, 573.2459).

Sarcglabtene L (12). white amorphous solid; $[\alpha]_D^{25} = -60.3$ ($c = 0.10$ in MeOH); ¹H and ¹³C NMR data, see Table S10; IR: $\nu_{\text{max}} = 3394, 2921, 2850, 1766, 1731, 1667, 1440, 1203, 1139, 923, 800, 725 \text{ cm}^{-1}$; UV (MeOH): λ_{max} (log ϵ) = 211 (1.32) nm; CD (MeOH): λ ($\Delta \epsilon$) = 204 (4.81), 220 (−1.96), 243 (1.24) nm; (+)-HRESIMS: m/z 543.1990 [M + Na]⁺ (calcd for C₃₀H₃₂O₈Na, 543.1989).

ECD Calculation. The calculations were performed by using the density functional theory (DFT) as carried out in the Gaussian 09. The preliminary conformational distributions search was performed using Yifuyun, and afforded stable conformers for compounds. Further geometrical optimization was performed at the B3LYP/6–31+G(d,p) level. Solvent effect of methanol solution was evaluated at the same DFT level by using the SMD method. TDDFT at B3LYP/6–311+G(d,p) was employed to calculate the electronic excitation energies and rotational strengths in methanol.

X-ray Crystallographic Data for 5 and 6. Crystal data were obtained on a Bruker APEX-II CCD, Bruker D8 VENTURE dual wavelength Mo/Cu, and Bruker D8 Venture detector using Cu κ -radiation ($\lambda = 1.54178 \text{ \AA}$) for **5** and **6**, respectively (Tables S12 and S13). The structures were solved by direct methods (SHELXS-97) and refined using full-matrix least-squares difference Fourier techniques. Hydrogen atoms bonded to carbons were placed on the geometrically ideal positions by the “ride on” method. Hydrogen atoms bonded to oxygen were located by the difference Fourier method and were included in the calculation of structure factors with isotropic temperature factors. Crystallographic data for **5** and **6** have been deposited with the Cambridge Crystallographic Data Centre (CCDC: 2435061–2435062).

Cell Culture. Human MDA-MB-231, HCT116, A549, MCF-7, HepG2 cells were cultured in a DMEM medium (Gibco, USA) including 10% fetal bovine serum (MiniGene, USA) and 1% penicillin/streptomycin (P/S) (Beyotime, China) at 37 °C with 5% CO₂.

Cytotoxicity Bioassay. The cells were seeded into 96-well culture plates (3.0×10^3 cells per well), and were treated with different concentrations of each compound for 48 h. MTT (5 mg/mL) was dissolved in PBS and sterile filtered, then 20 μL of the prepared solution was added to each well and cells were incubated for 4 h. The formed formazan crystals were dissolved in DMSO (150 μL /well) by constant shaking for 10 min at 25 °C. The absorbance was measured on a microplate reader (SpectraMax Plus384, Molecular Devices) at a test wavelength of 570 nm and a reference wavelength of 630 nm. In each experiment, three replicates of wells were prepared for each sample. The ratio of the living cells was determined by the difference in the absorbance between those of samples and controls. These differences were expressed in percentage, and cytotoxic activity was

indicated as an IC₅₀ value. *cis*-Diammineplatinum dichloride (DDP, CAS: 15663-27-1; Sigma, U.S.A) is the positive control.

Flow Cytometric Analysis. MDA-MB-231 cells were seeded into 6-well plates at a density of 1×10^6 cells/well and were treated with a series of 4 concentrations (0 and 5 μM) for 48 h. The cells were collected, washed in PBS, and resuspended in a 500 μL mixture of 5 μL Annexin V-FITC (Annexin V-PE) and 10 μL propidium iodide (7-AAD; MultiSciences Biotech, Co., Ltd.). BD Accuri C6 and FlowJo V10 software were employed to analyze the cell apoptosis data, respectively. At least 10,000 events were counted for each sample.

Western Blotting. MDA-MB-231 cells were divided into 4 groups: Control, compound **4** (1.25 μM), compound **4** (2.5 μM), and compound **4** (5 μM). The treatment groups were preincubated with corresponding compounds for 48 h. Total protein samples were extracted by RIPA buffer containing protease and phosphatase inhibitors. The concentrations of protein were determined by a BCA Kit. Approximately 60 μg of protein was then separated by 10% polyacrylamide gels, and transferred onto PVDF membranes. Following blocked in 5% lipid-free milk solution, the membranes were incubated with primary antibodies reactive to Erk, p-Erk, MEK, p-MEK, JNK, p-JNK, p38, p-p38, caspase 3, cleaved-caspase 3, caspase 9, cleaved-caspase 9, PARP, cleaved-PARP, Bax, BCL-2, GAPDH, and subsequently with secondary antibodies. Finally, the membranes were visualized with the ECL kit and analyzed by ImageJ software.

Cellular Thermal Shift Assay (CETSA) Analysis. Total cellular proteins of MDA-MB-231 were extracted after 48 h of compound treatment (**4**: 4 μM) using RIPA lysis buffer, and the blank group was treated with an equal amount of DMSO as the compound. The lysates were then divided equally into 10 portions and each group was heated with a thermal cycler at different temperatures (42, 44, 46, 48, 50, 52, 54, 56, 58, 60 °C) for 3 min, respectively. Then, the tubes were repeatedly frozen and thawed in liquid nitrogen for several times, and the supernatant was centrifuged. The supernatant was centrifuged, and 4x sampling buffer was added and boiled for 10 min before Western blot analysis.

DARTS Assays. Cells were washed with ice-cold PBS and then total protein samples were extracted by RIPA buffer containing protease and phosphatase inhibitors. The protein lysates were mixed with 10× TNC buffer (500 mmol/L Tris-HCl, pH = 8.0, 500 mmol/L NaCl and 100 mmol/L CaCl₂). The lysates in 1× TNC buffer were incubated with DMSO or compound **4** for 1 h at room temperature. Following the incubation, each sample was proteolyzed in various concentrations of Pronase (Roche Diagnostics, 10165921001) for 10 min at room temperature. After 10 min, 2 μL of ice-cold 20× protease inhibitor cocktail was added to stop proteolysis, and the samples were immediately placed on ice. Digestion was further stopped by adding 5× sample loading dye and boiling at 95 °C for 10 min. An equal portion of each sample was then loaded onto SDS-PAGE gels for Western blotting.

Cell Scratch Assays. For the scratch wound assay, 3×10^5 cells/well (three replicates per group) were plated into a 6-well plate and incubated to reach confluence. The monolayer was scratched using a tip and washed with serum-free medium to remove detached cells. Then the cells were cultured in serum-free medium supplemented with 4 (1, 2, 4 μM). HMECs were photographed at 0 h, 18 h and/or 36 h postwounding.

Molecular Docking. Molecular docking was used to confirm the binding of active components to key targets. We used AutoDock Vina 1.1.2 for semiflexible docking with 78% accuracy. The small molecule was the ligand, and Erk 1 (PDB: 4QTB) and 2 (PDB: 3ISZ) protein were the receptor. PyMOL 4.3.0 (<https://pymol.org/>) was used to prepare the structures. AutodockTools (<http://mgltools.scripps.edu/downloads>) were used for hydrogenation, charge checking, atom type designation, Gasteiger calculation, and grid box setup. The ligand's root and reversible bond were set in AutodockTools. Structures were converted to “PDBQT” for docking. LibDockScore were calculated, and interactions were analyzed and visualized using Discovery Studio.

Statistical Analysis. Statistical analysis was performed with Student's *t* test by using GraphPad Prism version 8.0.1 (GraphPad

Software, San Diego, CA). The data have been presented as the mean \pm standard deviation ($x \pm SD$). Generally, all experiments were carried out with $n \geq 3$ biological replicates. $P < 0.05$ was statistically significant.

■ ASSOCIATED CONTENT

Data Availability Statement

The NMR data for compounds 1–12 have been deposited in the Natural Products Magnetic Resonance Database (www.npmrd.org). The accession numbers are NP0351330 (Sarcglabtene A), NP0351331 (Sarcglabtene B), NP0351332 (Sarcglabtene C), NP0351333 (Sarcglabtene D), NP0351334 (Sarcglabtene E), NP0351335 (Sarcglabtene F), NP0351336 (Sarcglabtene G), NP0351337 (Sarcglabtene H), NP0351338 (Sarcglabtene I), NP0351339 (Sarcglabtene J), NP0351340 (Sarcglabtene K) and NP0351341 (Sarcglabtene L).

■ Supporting Information

The Supporting Information is available free of charge at <https://pubs.acs.org/doi/10.1021/acs.jnatprod.5c00785>.

^1H NMR and ^{13}C NMR data for 1–12; key 2D correlations of 2–4, 10, and 11; streptavidin-treated cell lysates were administered and analyzed, and then stained with Coomassie blue to identify the presence of proteins that may bind to 4; quantifications of MAPK pathway-related proteins expression after 4 treatment; quantifications of EMT-related proteins expression after 4 treatment; quantifications of apoptosis-related proteins expression after 4 treatment; quantifications of DARTS-related proteins expression after 4 treatment; binding free energy value of 4 to Erk receptor protein determined by Discovery Studio software; original 1D and 2D NMR, HRESIMS, IR, and CD spectra of 1–12 and full scans of Western Blot films for data in Figure 8C, 8D, 8F, 8G, and 8H (PDF)

Accession Codes

Deposition Numbers 2435061–2435062 contain the supplementary crystallographic data for this paper. These data can be obtained free of charge via the joint Cambridge Crystallographic Data Centre (CCDC) and Fachinformationszentrum Karlsruhe Access Structures service.

■ AUTHOR INFORMATION

Corresponding Authors

Lingyi Kong – Basic Medical Research Innovation Center for Anti-Cancer Drugs, MOE and Jiangsu Key Laboratory of Bioactive Natural Product Research, China Pharmaceutical University, Nanjing 211198, China;  orcid.org/0000-0001-9712-2618; Email: lykong@cpu.edu.cn

Jun Luo – Basic Medical Research Innovation Center for Anti-Cancer Drugs, MOE and Jiangsu Key Laboratory of Bioactive Natural Product Research, China Pharmaceutical University, Nanjing 211198, China;  orcid.org/0000-0002-7892-011X; Email: luojun@cpu.edu.cn

Authors

Danyang Zhang – Basic Medical Research Innovation Center for Anti-Cancer Drugs, MOE and Jiangsu Key Laboratory of Bioactive Natural Product Research, China Pharmaceutical University, Nanjing 211198, China

Zhiqi Xiao – Basic Medical Research Innovation Center for Anti-Cancer Drugs, MOE and Jiangsu Key Laboratory of

Bioactive Natural Product Research, China Pharmaceutical University, Nanjing 211198, China

An Huang – Basic Medical Research Innovation Center for Anti-Cancer Drugs, MOE and Jiangsu Key Laboratory of Bioactive Natural Product Research, China Pharmaceutical University, Nanjing 211198, China

Pengfei Tang – Basic Medical Research Innovation Center for Anti-Cancer Drugs, MOE and Jiangsu Key Laboratory of Bioactive Natural Product Research, China Pharmaceutical University, Nanjing 211198, China

Houli Jiang – Basic Medical Research Innovation Center for Anti-Cancer Drugs, MOE and Jiangsu Key Laboratory of Bioactive Natural Product Research, China Pharmaceutical University, Nanjing 211198, China

Mengmeng Yu – Basic Medical Research Innovation Center for Anti-Cancer Drugs, MOE and Jiangsu Key Laboratory of Bioactive Natural Product Research, China Pharmaceutical University, Nanjing 211198, China

Ze Zheng – Basic Medical Research Innovation Center for Anti-Cancer Drugs, MOE and Jiangsu Key Laboratory of Bioactive Natural Product Research, China Pharmaceutical University, Nanjing 211198, China

Complete contact information is available at:
<https://pubs.acs.org/10.1021/acs.jnatprod.5c00785>

Funding

This work was financially supported by the Basic Research Project for the Development of Modern Industrial College of Traditional Chinese Medicine and Health at Lishui University.

Notes

The authors declare no competing financial interest.

■ ACKNOWLEDGMENTS

This research was supported by the National Natural Science Foundation of China (32070389, 82430118), the Double First Class University Project of China Pharmaceutical University (CPU2022QZ29), the 111 Project from Ministry of Education of China (B18056), and Postgraduate Research & Practice Innovation Program of Jiangsu Province (KYCX25_1063).

■ REFERENCES

- (1) Atanasov, A. G.; Zotchev, S. B.; Dirsch, V. M.; International Natural Product Sciences; Supuran, C. T.; et al. *Nat. Rev. Drug. Discovery* **2021**, *20*, 200–216.
- (2) Luo, Z. W.; Yin, F. C.; Wang, X. B.; Kong, L. Y. *Chin. J. Nat. Med.* **2024**, *22*, 195–211.
- (3) Luo, J.; Zhang, D. Y.; Tang, P. F.; Wang, N.; Zhao, S.; Kong, L. Y. *Nat. Prod. Rep.* **2024**, *41* (1), 25–58.
- (4) Sun, Y. P.; Chi, J.; Zhang, L.; Wang, S. Y.; Chen, Z. H.; Zhang, H.; Kong, L. Y.; Luo, J. *J. Org. Chem.* **2022**, *87*, 4323–4332.
- (5) Bai, M.; Liu, Y.-Y.; Li, Y.-L.; Shi, W.-Y.; Li, K.-X.; Lu, L.-W.; Le Zhou; Bin Lin; Huang, X.-X.; Song, S.-J. *Ind. Crops Prod.* **2022**, *183*, 114983.
- (6) Wu, X. J.; Cao, D.; Chen, F. L.; Shen, R. S.; Gao, J.; Bai, L. P.; Zhang, W.; Jiang, Z. H.; Zhu, G. Y. *ACS. Omega.* **2022**, *7*, 35063–35068.
- (7) Wen, J.; Yu, M. M.; Jiang, H. L.; Zhu, Y.; Zhang, D. Y.; Yang, M. Z.; Kong, L. Y.; Luo, J. *Bioorga. Chem.* **2025**, *158*, 108327.
- (8) Cui, Z. R.; Wang, Y. Y.; Li, J. X.; Chi, J.; Zhang, P. P.; Kong, L. Y.; Luo, J. *Org. Lett.* **2022**, *24*, 9107–9111.
- (9) Wang, X. J.; Xin, J. L.; Xiang, H.; Zhao, Z. Y.; He, Y. H.; Wang, H. B.; Mei, G. Y.; Mao, Y. C.; Xiong, J.; Hu, J. F. *Chin. Chem. Lett.* **2024**, *35*, 109682.

- (10) Wu, Z. Y.; Peter, H. R.; Hong, D. Y. *Flora of China*; Science Press, 1999; p 132.
- (11) Wang, Y. Y.; Li, Q. R.; Chi, J.; Li, J. X.; Kong, L. Y.; Luo, J. *Chin. J. Nat. Med.* **2022**, *20*, 215–220.
- (12) (a) Berova, N.; Ellestad, G. A.; Harada, N. *Comprehensive Natural Products II Chemistry and Biology*. **2010**, *9*, 91–146.
(b) Zhang, D. Y.; Xiao, Z. Q.; Wang, N.; Huang, A.; Wen, J.; Kong, L. Y.; Luo, J. *Bioorga. Chem.* **2024**, *146*, 107259.
- (13) Zhan, Z. C.; Xia, Y. P.; Tang, Q.; Zhu, H. H.; Du, J. Y.; Cai, J. X.; Chen, Y. J.; Wu, Z. N.; Li, Y. L.; Chen, N. H.; Wang, G. C.; Zhang, Y. B. *Phytochem.* **2023**, *215*, 113859.
- (14) Wong, K. C.; Tan, M. S.; Ali, D. M. H.; Teoh, S. G.; Osman, H.; Tan, S. K. *J. Essent. Oil Res.* **2009**, *21*, 71–73.
- (15) Flack, H. D.; Bernardinelli, G. *Chirality* **2008**, *20*, 681–690.
- (16) Sun, Y. P.; Wang, Y. Y.; Li, Y. Y.; Wang, S. Y.; Zhang, D. Y.; Kong, L. Y.; Luo, J. *Org. Biomol. Chem.* **2022**, *20* (46), 9222–9227.
- (17) Chi, J.; Wei, S. S.; Gao, H. L.; Xu, D.; Zhang, L.; Yang, L.; Xu, W. J.; Luo, J.; Kong, L. Y. *J. Org. Chem.* **2019**, *84* (14), 9117–9126.
- (18) Zhu, W. F.; Guo, S.; Shi, J. L.; Song, K.; Yu, Y.; Tan, R.; Lou, S. R.; Chen, J.; Qiao, L. P.; Hu, M. *Environ. Sci. Technol. Lett.* **2024**, *11* (10), 1068–1074.
- (19) Lewis, J. B.; Hedrick, G. W. *J. Org. Chem.* **1965**, *30*, 4271–4275.
- (20) Li, J. X.; Chi, J.; Tang, P. F.; Sun, Y. P.; Lu, W. J.; Xu, W. J.; Wang, Y. Y.; Luo, J.; Kong, L. Y. *Chin. J. Chem.* **2022**, *40*, 603–608.
- (21) Li, C. J.; Zhang, D. M.; Luo, Y. M.; Yu, S. S.; Li, Y.; Lu, Y. *Phytochem.* **2008**, *69*, 2867–2874.
- (22) Liu, X.; Fu, J.; Yang, J.; Huang, A. C.; Li, R. F.; Bai, L. P.; Liu, L.; Jiang, Z. H.; Zhu, G. Y. *ACS. Omega.* **2021**, *6* (8), 5898–5909.
- (23) Li, J. X.; Cui, Z. R.; Li, Y. Y.; Han, C. H.; Zhang, Y. Q.; Tang, P. F.; Cui, L. T.; Zhang, H.; Luo, J.; Kong, L. Y. *Chin. Chem. Lett.* **2022**, *33*, 4257–4260.
- (24) Chi, J.; Xu, W. J.; Wei, S. S.; Wang, X. B.; Li, J. X.; Gao, H. L.; Kong, L. Y.; Luo, J. *Org. Lett.* **2019**, *21*, 789–792.
- (25) Zhou, J. S.; Huang, S. L.; Gao, Y.; Liu, Q. F.; Leng, Y.; Zhou, B.; Yue, J. M. *J. Nat. Prod.* **2022**, *85*, 2090–2099.
- (26) Begley, M. J.; Fish, P. V.; Pattenden, G.; Hodgson, S. T. *J. Chem. Soc., Perkin Trans.* **1990**, *1*, 2263–2271.
- (27) Zeng, Y. L.; Liu, J. Y.; Zhang, Q.; Qin, X. H.; Li, Z. L.; Sun, G. J.; Jin, S. R. *Front. Pharmacol.* **2021**, *12*, 652926.
- (28) Fang, J. Y.; Richardson, B. C. *Lancet Oncol.* **2005**, *6*, 322–327.



CAS BIOFINDER DISCOVERY PLATFORM™

ELIMINATE DATA SILOS. FIND WHAT YOU NEED, WHEN YOU NEED IT.

A single platform for relevant, high-quality biological and toxicology research

Streamline your R&D

CAS
A division of the
American Chemical Society